



Numerical Simulation of the Reorientation Process Under Different Conditions in a Vane-type Surface Tension Propellant Tank

Lu Wang¹ · Xiangyun Zhang¹ · Yinyin Yun¹ · Jintao Liu² · Wen Li² · Bin Huang¹

Received: 27 December 2021 / Accepted: 19 April 2022 / Published online: 31 May 2022
© The Author(s), under exclusive licence to Springer Nature B.V. 2022

Abstract

The fuel tank, as a significant component for the propellant system in satellites, plays an important role in managing propellant and maintaining stability through its propellant management device (PMD). To analyze the effect of propellant volume fill ratios and acceleration conditions on the fluid flow in vane-type surface tension tanks, this study carried out computational fluid dynamics (CFD) simulation with the Volume of Fluid (VOF) model. The four fill ratios are 5%, 25%, 50%, and 75%; the four acceleration environments are bottom acceleration, lateral acceleration, reverse acceleration, lateral & reverse acceleration, and rotation condition. First, the contour and the interface of gas and liquid were tracked to evaluate the ability of the PMD. Second, the volume flow rate through the initial interface of gas and liquid was monitored to judge the sloshing intensity in the reorientation process. At last, the force in different simulation conditions was analyzed to further research fluid sloshing intensity. The results show reorientation process in the vane-type surface tension tank can be divided into two stages: the mutational stage and the stable stage. The fill ratio and the acceleration condition influence the value and duration of the max flow rate through the initial interface, and further influence the sloshing intensity in the reorientation process. By comparing the results at lateral acceleration, reverse acceleration, and lateral & reverse acceleration with the same fill ratio, it can be found that the acceleration in the Z direction has a stronger influence on the reorientation process.

Keywords Microgravity · Vane-type surface tension tank · VOF model · Numerical simulation

Introduction

The fuel tank, as a core component in the propulsion system, is responsible for storing propellant, managing propellant, and transporting propellant to thrust chambers when it is needed (Hibbard 1996). The core component in the fuel tank is the propellant management device (PMD) (Jaekle 1997, 1991). According to the PMD type, fuel tanks can be classified into spin tanks, diaphragm tanks, and surface tension tanks. Among those tanks, surface tension tanks are most widely used (Zhuang et al. 2020). They separate the gas from the liquid through the PMD and deliver clean propellant to the outlet driven by liquid surface tension. By 1985,

more than 19 surface tension tanks had been designed by Lockheed Missiles & Space Company (LMSC), and 13 of them had been tested, which provided 4 important commercial designs for later communication satellites (Rollins et al. 1985).

According to the fluid mechanics of propellant management, PMDs can be classified into two categories: screen-based PMDs and vane-type PMDs (Hartwig 2016). The screen-based PMDs can meet the requirements of all accelerations in the microgravity environment, but they still have downsides. For example, they have short service lifespan and large mass. Therefore, the United States put forward the idea of vane-type surface tension tanks in the 1970s (Dowdy et al. 1977; Peterson 1976). They have simpler structures, fewer components, longer service lifespan and they are easier to carry. The configuration of the gas–liquid free boundary in vane-type surface tension tanks in the microgravity environment is a focus of study. In the low gravity environment of orbiting vehicles, the surface tension force is significant and often dictates the location and orientation of liquid within vessels, conduits, etc., which may be negligible in

✉ Bin Huang
binhuang@zju.edu.cn

¹ Ocean College, Zhejiang University, Zhoushan 316021, China

² Beijing Engineering Research Center of Efficient and Green Aerospace Propulsion, Technology, Beijing Institute of Control Engineering, Beijing 100094, China

the gravity environment. And in that environment, the shape of the gas–liquid free boundary is determined by geometric boundary conditions, surface tension force, contact angle, and residual acceleration produced by the environment (Jaekle 1991). The research about tracking gas–liquid free boundaries can be traced back to Laplace. The application of computers and the development of computational fluid dynamics (CFD) revived this study. Shooting Method, Runge–Kutta Method (Leon 1968), Adams–Bashforth Method (Michael 1981), Power-series Method (Stark et al. 1974), Rayleigh–Ritz Method (Dodge 1971) and CFD simulation (Liu et al. 2020; Thibaut et al. 2011) have been used to calculate the free boundary. There are two factors influencing the development of the gas–liquid free boundary: a) forced flow driven by pressure gradient; b) capillary flow in interior corners.

The research on pressure gradient driving flow was first studied by Jaekle (1991) using a simple vane which was defined as a thin solid sheet perpendicular to and traversing the boundary surface. Jaekle performed numerical model computations of a liquid flow through two communicating T-shaped capillary channels. For this model, solutions for interface shapes could not be computed for all flow rates. Jaekle attributed this phenomenon to the “choking effect”, i.e., a general flow rate limitation. Once the flow rate exceeds a certain value, the pressure difference between the liquid and the gas phase will no longer be balanced by the curvature of the free surface. Consequently, the free surface will lose its stability, which then will lead to gas collapsing, and then the gas will ingest into the flow path. Two phase flow caused by gas ingestion is unfavorable for certain applications (Bronowicki et al. 2015). Srinivasan (2003) proposed a semi-analytical procedure to accurately calculate the extremely small fuel flow rates under reasonably idealized conditions. Rosendahl et al. (Rosendahl et al. 2010) studied convective dominated flows in open capillary parallel-plate channels and introduced a method to determine the speed index. A general relation for the speed index, a function of the flow rate and the channel length has been found which clarifies the fundamental behavior of the choking effect. Bronowicki et al. (2015) experimentally and numerically investigated a forced flow through a partially open capillary channel focusing on the interface of steady flow with stable free surfaces. Wu et al. (2019) studied the forced flow through curved open capillary channels under microgravity conditions and concluded that the pressure loss and the centrifugal force effect are the causes of the maximum flow rate difference between the curved channel and the straight channel.

Capillary flows in interior corners are defined as spontaneous interfacial flows driven by surface tension, container geometry, and surface wettability, for which the impact of gravity is negligible (Chen et al. 2006). A wetting

phenomenon of fundamental importance was first described with mathematical rigor by Concus and Finn (1969). The Concus–Finn condition is a geometric wetting condition that corresponds to an underpressure in the liquid, which results in capillary-driven flow into and along the interior corner (Weislogel 2001). Lenormand and Zarcone (1984) calculated approximate laws for the flow rate by roughness and corners in an infinitely long square duct and built a theoretical model to describe the relationship between the fluid configuration and the flow rate. Dong and Chatzis (1995) studied the imbibition of wetting liquids in the corners of a square capillary tube under transient flow conditions from the perspective of the dimensionless flow resistance concept. Weislogel and Lichter (1998) studied the spontaneous redistribution of fluid along an interior corner of a container under the influence of capillary forces. Chen et al. (2006) (Kang et al. 2008) experimentally and numerically studied capillary flows along rounded interior corners. Wu et al. (2018) researched the capillary flows in curved interior corners and established a theoretical model to study the curved corner effects.

To ensure gas-free propellant delivery, PMDs in the propellant tank are designed to utilize surface tension forces which are significant in the low gravity environment. The Viking 75 was the world’s first flying plate surface tension tank. Jaekle (1997) proposed the conceptual design for PMD and analyzed its performance. The United States, Europe, Japan, and other space powers have adopted vane-type surface tension tanks in the main geostationary orbit satellite platform (Ibrahim et al. 2001; Tam et al. 2008). Wei et al. (2013) took the analytic and experimental methods to study the basic flow theory concluding the capillarity, the orientation process, the inflow process, and the exclusive of the propellant. Li et al. (2007) analyzed the vane-type surface tension tank from experimental research, numerical simulation, and actual application. They provided research about new satellite propellants with valuable references. Liu et al. (2020) took a microgravity drop tower test to study the influence of the geometry on the transport performance of a new vane-type propellant tank. Experimental results provided a favorable reference for further optimization design of vanes and refillable sponges.

Vane-type surface tension tanks work in the micro or zero gravity environment, where the fluid movement is complicated. And it is difficult to validate the performance of liquid movement on the ground. Therefore, numerical simulation becomes a significant way to study the internal flow mechanism. Several researches recommend the employment of the Volume of Fluid (VOF) model for numerical simulations about multiphase flows to track free fluid surfaces (Stuparu et al. 2021). The VOF model was first developed by Hirt and Nichols, from the American Los Alamo scientific LABS, to deal with the two-dimensional viscous fluid with free surface

simulation (Hirt and Nichols 1981). This model introduces a Fluid volume fraction α function to describe mixture density and configure complicated free boundaries. Many studies have been done to improve the accuracy and efficiency of the VOF model. (Albadawi et al. 2014; Gueyffier et al. 1999; Shin and Lee 2000). Veldman et al. (2007) investigated the influence of sloshing liquids in spacecraft and satellites with the improved VOF model which includes capillary surface physics as well as coupled solid–liquid interaction dynamics, and validated the reliability of the model. Kartuzova and Kassemi (2011) researched the pressurization of cryogenic storage tanks with both the Sharp Interface and the VOF approaches to represent the transfer of the phase boundary and the associated interfacial heat, mass, and momentum between the liquid and the vapor regions. Both models were validated against the microgravity pressurization data provided by the Saturn S-IVB AS-203 experiment with the VOF model, which presented a better agreement. In 2016, Kartuzova and Kassemi (2016) used the VOF model of the ANSYS Fluent CFD code again to model the jet mixing segments of TPCE tests, and validated the two phase CFD model against the experimental results. Silva et al. (Silva et al. 2020) employed OpenFOAM and ANSYS Fluent to study microscale gas–liquid flow. They assessed the capability of both software to predict the flow field by employing different models for the multiphase flow: VOF and piecewise linear interface calculation (PLIC) in ANSYS Fluent and MULES/iso Advector in OpenFOAM. The conclusion of the research, after validating the results obtained from experimental data, is that ANSYS Fluent provides more accurate results for this type of flow.

When the aircraft is under operation, it is impossible to ignore sloshing problems of fluids in tanks. A larger

sloshing behavior will produce a greater interference force, interference torque, and impact pressure on the spacecraft. In severe cases, it will cause instability of the control system or structural damage (Hu et al. 2017). NASA has taken the lead in theoretical research on the dynamics of liquid sloshing since the 1960s. Abramson (Rollins et al. 1985) has come up with a comprehensive and systematic theoretical solution to the small lateral sloshing of liquids in several special-shaped containers, such as rectangular and cylindrical shapes. Yang and Peugeot (2014) used CFD to estimate the sloshing resonance frequency and sloshing quality of various tanks in the basic sloshing mode. Huang et al. (2021) studied the propellant sloshing behavior in a vane-type surface tension tank in the lateral microgravity environment by the VOF model. Saltari et al. (2021) proposed Reduced-Order Models (ROMs) based on data provided by CFD simulations for generally flexible tanks to be embedded in a larger aerospace structure.

Even though much research about microgravity flow in vane-type tanks has been done, the effect of the different work conditions has not been analyzed, which is instructive for the design of the vane-type tank. Thus, this study simulated the reorientation process with different liquid volume fill ratios in different acceleration environments and carefully researched the difference between them. A new vane-type tank is designed in this study. Commercial software Ansys Fluent with the VOF model was used to simulate different conditions. The volume flow rate through the initial gas–liquid interface and the distribution of gas and liquid was monitored to analyze the reorientation process. The force during different reorientation processes was compared to get the specific effect of the acceleration environments and liquid fill ratios.

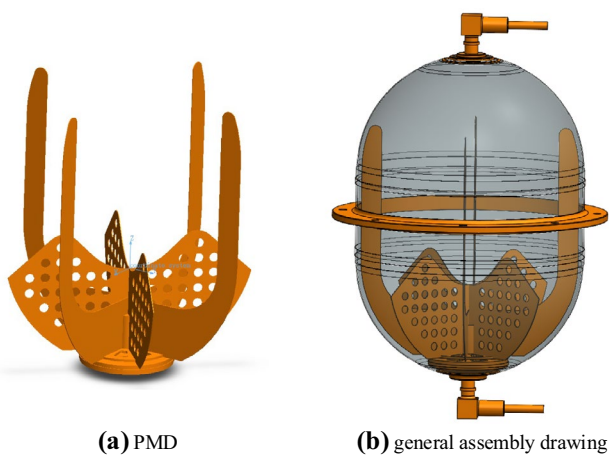


Fig. 1 Structure of vane-type surface tension propellant tank



Fig. 2 Simplified model

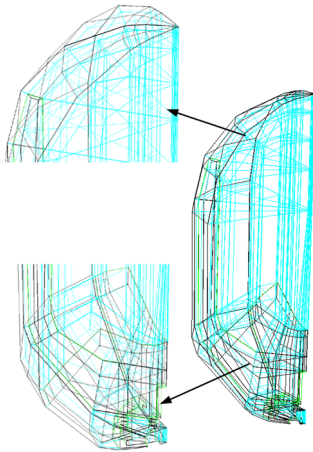


Fig. 3 The topological structure of the quarter tank

Geometry

Propellant Tank

The studied vane-type surface tension propellant tank consists of an upper hemisphere, a middle cylinder, and a lower hemisphere. The radiuses of the hemisphere and the cylinder are 85 mm, and the height of the cylinder is 71.2337 mm. The total volume of the tank is 4L. The vane-type PMD in this tank has 4 vanes and a sponge device made up of 4 panels. The vane-type PMD provides gas-free propellant delivery by establishing a communication path between the bulk of the propellant and the sponge device (Jaekle 1991). The sponge device is an open structure that holds and provides a specific quantity of propellant using surface tension forces, and it is refillable (Jaekle 1993). The 4 vanes are arranged in the +X, -X, +Y, and -Y directions acting as a transporter of the propellant. The 4 panels are interleaved with the vanes acting as a reservoir of the propellant. The structure of the PMD is shown in Figure 1(a) and the whole tank is shown in Figure 1(b).

Computation Domain

As the geometry of the vane-type surface tension propellant tank is complicated, it is needed to simplify the initial geometry to make the simulation easier and faster. In this study, the vane-type tank is the study core rather than

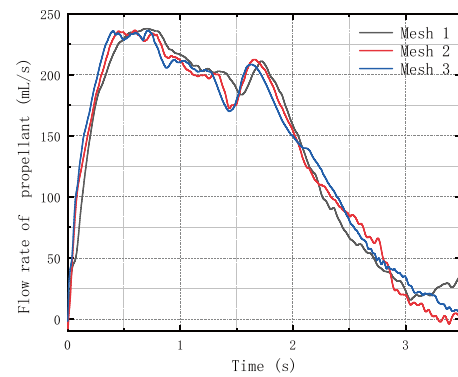


Fig. 4 Mesh independence study

the system, so the inlet pipe and the outlet pipe are unnecessary. The geometry of the sponge of the study tank has holes that were not designed in early design (Dowdy et al. 1977; Jaekle 1993). The reason why plates are perforated is to reduce the mass of the PMD, but this also leads to a less efficient device. The propellant acquisition can be greatly reduced and vapor ingestion can thus become an issue with the increase of the size and the quantity of the holes. Therefore, sponge mass is often traded with performance to determine the optimal design for particular missions (Hartwig 2017). As the holes will decrease the size of the element and increase the number of the element, the holes are ignored to better show the ability of the sponge and decrease the simulation time. The simplified model used in the numerical simulation is shown in (Fig. 2).

Computational Method and Simulation Condition

Computational Model

The numerical simulation is conducted with the commercial software Ansys Fluent (ANSYS 2012) with the VOF model. In the VOF method, a volume fraction is defined in each cell in a way that the volume fractions of all the phases sum to unity. In the cell, the change in the interface can be tracked by solving a continuity equation for the volume fraction of each phase (Kartuzova and Kassemi 2011). As the Reynolds number of the propellant flows in the tank under micro-gravity is small, the flow is treated as laminar flow.

Table 1 Mesh details

Mesh No	Number of Nodes	Number of Faces	Number of Elements
Mesh 1(Corse)	4,126,871	12,191,108	4,031,916
Mesh 2(Median)	6,585,052	19,510,280	6,462,336
Mesh 3(Fine)	11,086,816	32,651,708	10,828,500

Table 2 Physical parameters for simulation

Name	Molecular formula	ρ (kg/m ³)	μ (Pa•S)	Contact angle (°)	σ (N/m)
helium	He (gas)	0.1625	1.99×10^{-5}	5	0.0698
hydrazine anhydrous	H ₄ N ₂ (liquid)	1008	9.35×10^{-4}		

The fundamental equations for this study are as follows:

$$\frac{\partial}{\partial t}(\rho) + \frac{\partial}{\partial x_i}(\rho u_i) = 0 \tag{1}$$

$$\frac{\partial \alpha}{\partial t} + \frac{\partial}{\partial x_i}(\alpha u_i) = 0 \tag{2}$$

$$\rho = \alpha \rho_1 + (1 - \alpha) \rho_2 \tag{3}$$

$$\frac{\partial}{\partial t} \rho u_j + \frac{\partial}{\partial x_i} \rho u_i u_j = - \frac{\partial p}{\partial x_j} + \mu \frac{\partial}{\partial x_i} \left(\frac{\partial u_i}{\partial x_j} + \frac{\partial u_j}{\partial x_i} \right) + \rho g + F_{vol} \tag{4}$$

where, ρ is the mixture density; u is the velocity of the mixture; x is the coordinate; subscripts i and j are directions of Cartesian coordinates; α is the volume fraction of gas; ρ_1 is the density of the gas; ρ_2 is the density of the liquid; p is the static pressure; t is time; g is the gravitational acceleration; μ is the dynamic viscosity of the mixture which can be calculated with the same method as density; F_{vol} is the volume force.

In this study, the surface tension forces at the interface are modeled via the Continuum Surface Force (CSF) model proposed by Brackbill et al. (1992). In this model, the surface tension forces at the interface are transformed into a volume force:

$$F_{vol} = \sigma \frac{\rho \kappa \nabla \alpha}{\frac{1}{2}(\rho_1 + \rho_2)} \tag{5}$$

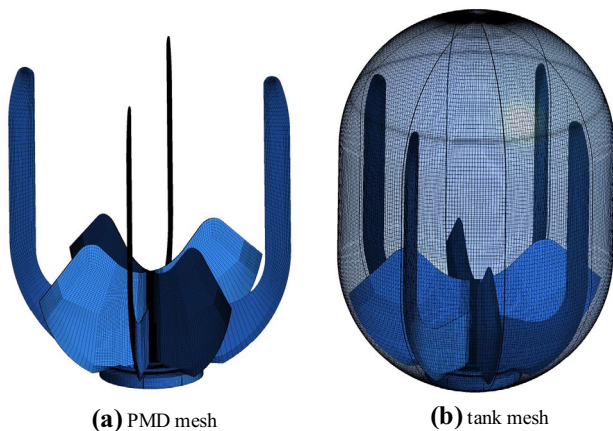


Fig. 5 Simulation mesh

$$\kappa = \nabla \cdot \frac{(\nabla \alpha)}{|\nabla \alpha|} \tag{6}$$

where, σ is the surface tension coefficient; κ is the interface curvature in terms of the divergence of the unit normal.

Mesh Independence

A mesh independence test was conducted with the reorientation process at 50% fill ratio under the bottom condition (i.e. $2 \times 10^{-3} g_0$ at Z direction). Ansys ICEM was used to mesh the tank. As this vane-type tank is an axisymmetric geometry, the topological structure was only divided in the quarter geometry, which is shown in (Fig. 3). The total structure can be acquired by rotating and copying the quarter structure. Changing the number of nodes in the Z direction, three grids were gotten, the details of which are listed in Table 1. The volume flow rates through initial gas–liquid interfaces (shown in Fig. 6) were monitored. As the reorientation is a long period process, the time when the flow rate of any mesh first gets zero is chosen as the end time. The simulation results are shown in (Fig. 4). It can be found

Table 3 The conditions for simulation

Simulation No	Acceleration environment	Fill ratio
1	X=0 g ₀	5%
2	Y=0 g ₀	25%
3	Z=2×10 ⁻³ g ₀	50%
4	Rotation velocity=0 °/s	75%
5	X=0 g ₀	5%
6	Y=2×10 ⁻³ g ₀	25%
7	Z=0 g ₀	50%
8	Rotation velocity=0 °/s	75%
9	X=2×10 ⁻³ g ₀	5%
10	Y=0 g ₀	25%
11	Z=-2×10 ⁻³ g ₀	50%
12	Rotation velocity=0 °/s	75%
13	X=0 g ₀	5%
14	Y=0 g ₀	25%
15	Z=-2×10 ⁻³ g ₀	50%
16	Rotation velocity=0 °/s	75%
17	X=0 g ₀	5%
18	Y=0 g ₀	25%
19	Z=0 g ₀	50%
20	Rotation velocity=5 °/s	75%

from (Fig. 4), the flow rate curve trends of the three grids are similar, except for some differences among the three curves. Compared with the flow rate curves of mesh 2 and mesh 3, the flow rate curve of mesh 1 is smoother, which means many details could not be tracked by mesh 1. Besides, when the flow rate of mesh 2 and mesh 3 get to zero, the flow rate of mesh 1 is still not. As the calculation results of mesh 2 and mesh 3 are similar, mesh 2 is considered as the mesh independency to save the simulation time. Subsequent simulations are performed with the meshing scheme of mesh 2 which is shown in (Fig. 5).

Simulation Condition

The computational domain contains two phases: the primary phase is the helium (gas), and the secondary phase is the hydrazine anhydrous (liquid). The density and dynamic viscosities of the liquid are respectively taken to be $\rho_l = 1008\text{kg/m}^3$, $\mu_l = 9.35 \times 10^{-4}\text{Pa} \cdot \text{S}$, corresponding to hydrazine anhydrous at 20 °C. The density and dynamic viscosities of the gas are respectively taken to be $\rho_g = 0.1625\text{kg/m}^3$, $\mu_g = 1.99 \times 10^{-5}\text{Pa} \cdot \text{S}$. The surface tension factor σ between helium (gas) and hydrazine anhydrous (liquid) is 0.0698N/m .

Table 4 Gas–liquid contours under different conditions

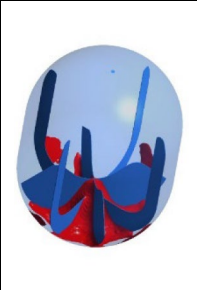












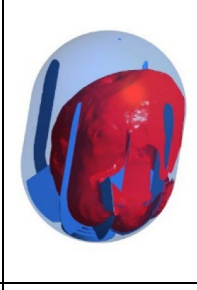
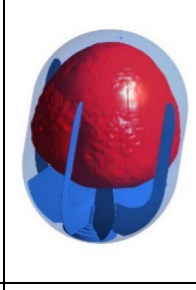




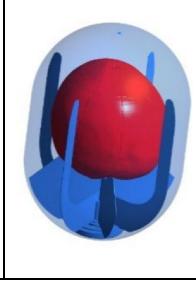
Fill ratio	Bottom condition	Lateral condition	Reverse condition	Lat-rev condition	Rotation condition
5%					
25%					
50%					
75%					

The Physical parameters for simulation are listed in Table 2. Every wall was set to no penetrate and no slip wall boundary condition. The time-dependent Navier–Stokes equations were applied to resolve the flow inside the propellant tank and the time step was chosen to be 0.0001 s to get better convergence.

According to the microgravity environment of the on-orbit aircraft, this study simulates 5 kinds of acceleration environments and 4 kinds of fill ratios to figure out the different effects of different acceleration environments and different propellant volume fill ratios during the reorientation process. The simulation conditions are listed in Table 3,

g_0 is the gravitational acceleration and the rotation axis is Z-axis. Simulation No.1 to No.4 simulated the bottom acceleration ($2 \times 10^{-3} g_0$ in the Z direction); simulation No.5 to No.8 simulated the lateral acceleration ($2 \times 10^{-3} g_0$ in the Y direction); simulation No.9 to No.12 simulated the lateral & reverse acceleration ($2 \times 10^{-3} g_0$ in the minus Z direction and $2 \times 10^{-3} g_0$ in the X direction); simulation No.13 to No.16 simulated the reverse acceleration ($2 \times 10^{-3} g_0$ in the minus Z direction); simulation No.17 to No.20 simulated the rotation condition (the rotation speed is $5^\circ/s$ and rotation axis is Z-axis). Based on the propellant volume fill ratio and the

Table 5 Gas-liquid interface under different conditions

Fill ratio	Bottom condition	Lateral condition	Reverse condition	Lat-rev condition	Rotation condition
5%					
25%					
50%					
75%					

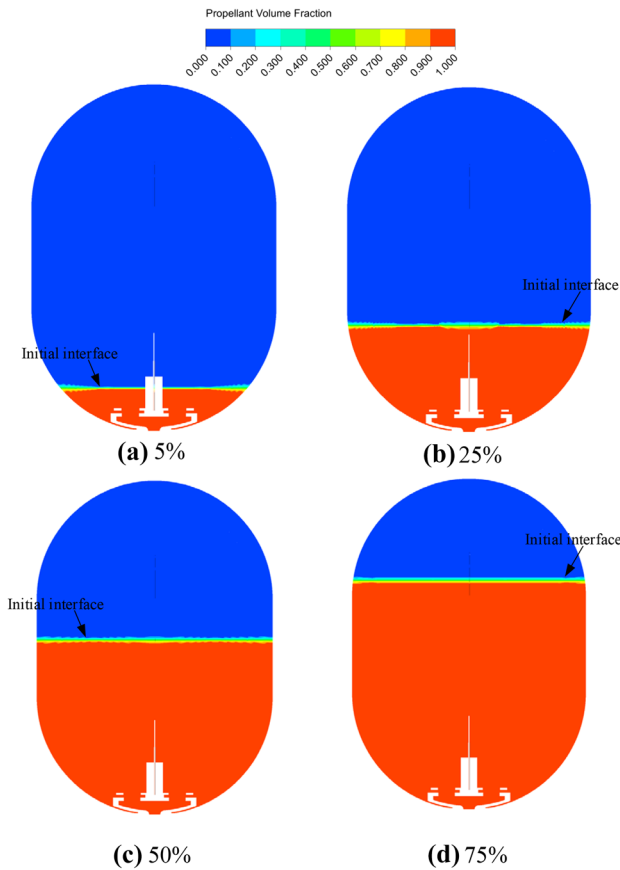


Fig. 6 Initial gas–liquid contours

volume of the tank, the specific height of the liquid was calculated. The Initial gas–liquid contour and initial gas–liquid interface of different fill ratios are shown in (Fig. 6).

Result and Discussion

Final fluid form under different conditions

The reorientation processes at the bottom acceleration, the lateral acceleration, the lateral & reverse acceleration, the reverse acceleration, and the rotation condition with different fill ratios have been simulated. During the calculation, the instantaneous volume flow rate through the initial gas–liquid interface and instantaneous mass center of the liquid along the Z-axis were monitored. The mass center has been uniformized to clearly show the relative height of the mass to the tank. When the reorientation process is completed, a stable liquid level can be observed: the volume flow rate of the initial gas–liquid interface becomes stable to zero, and the mass center of the liquid keeps constant. The whole reorientation process always keeps a long period, and the oscillatory convergence process always takes up a lot of the reorientation time. However, the oscillatory convergence process is not significant in terms of the total process. So, the state closed to the converge is chosen as reorientation completion even though it would keep slightly oscillating for a while. Table 4 shows the snapshots of the gas–liquid contour (red stands for the liquid, and blue stands for the gas), and Table 5 shows the gas–liquid interface at the instant of reorientation completion for different conditions. From every row of Tables 4 and 5, different final forms under the effect of different acceleration environments can be compared clearly. And from every column of Tables 4 and 5, different final forms under the effect of different fill ratios can be compared clearly.

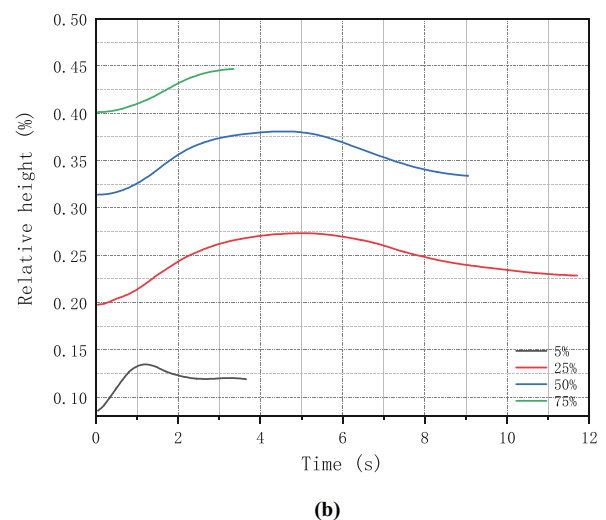
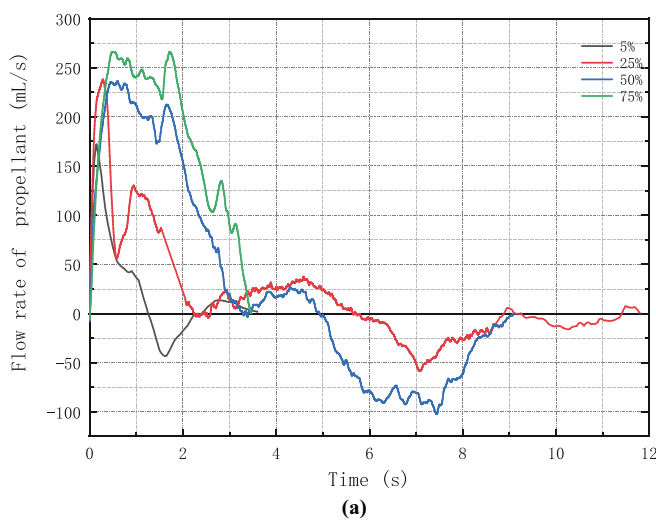


Fig. 7 Flow rate curve and mass center curve under bottom acceleration

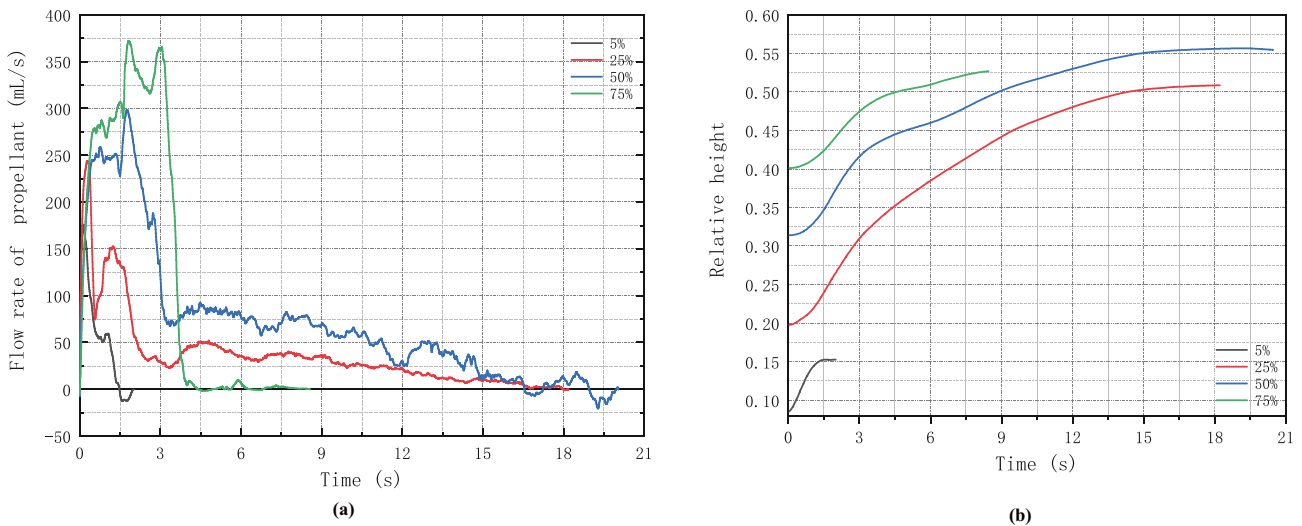


Fig. 8 Flow rate curve and mass center curve under reverse acceleration

Because of the surface tension effect, the liquid mainly transfers in the gap between the vanes and the inner wall of the tank which has been studied by Jaekle (1991). Through comparing the contour and the interface of different fill ratios in the same accelerate environment, it can be found that when the fill ratio is higher, the air cavity will be more completed. With the acceleration environment changing, the location and the shape of the gas cavity change a lot, which will become conspicuous when the propellant fill ratio is large. Besides the fill ratio and the acceleration environment, the boundary shape of the air cavity is also influenced by the vanes. When the propellant fill ratio is small or the

propellant is close to the vanes, the propellant flows mainly along the vanes, which affects the edge form of the air cavity a lot. As for the rotation condition, the gas–liquid interface is smoother compared with other accelerate conditions, which may be caused by the high angular acceleration.

Transfer Process Between Different Conditions

To figure out the specific influence of the propellant fill ratio and the acceleration environment during the reorientation process, the flow rate/time curve and the mass center/time curve are put side by side. From the flow rate/

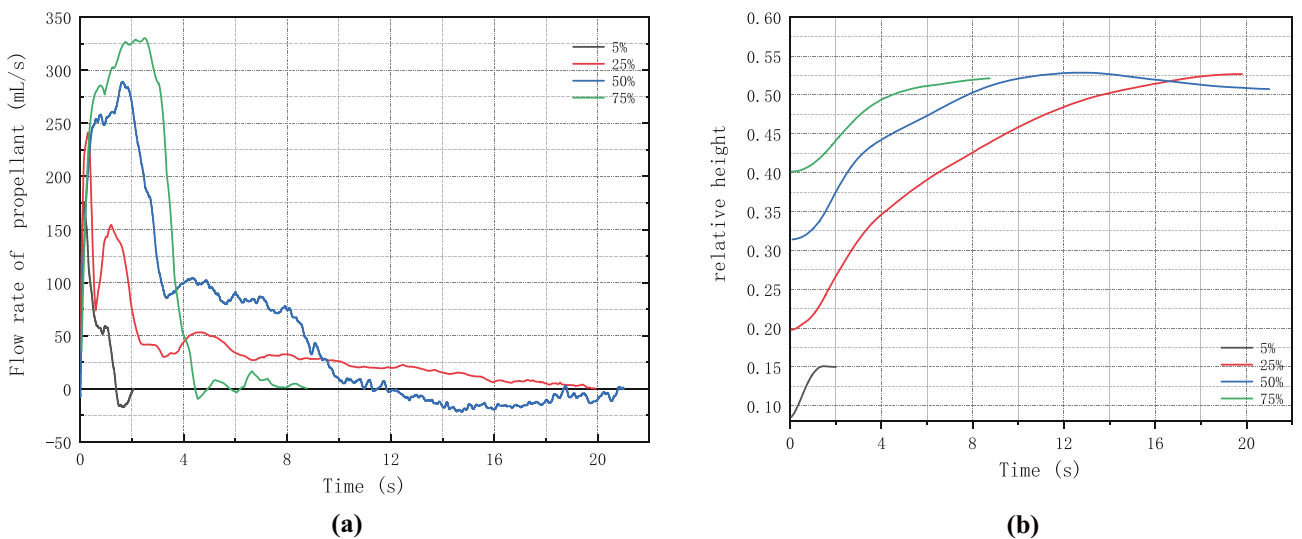


Fig. 9 Flow rate curve and mass center curve under Lateral&reverse acceleration

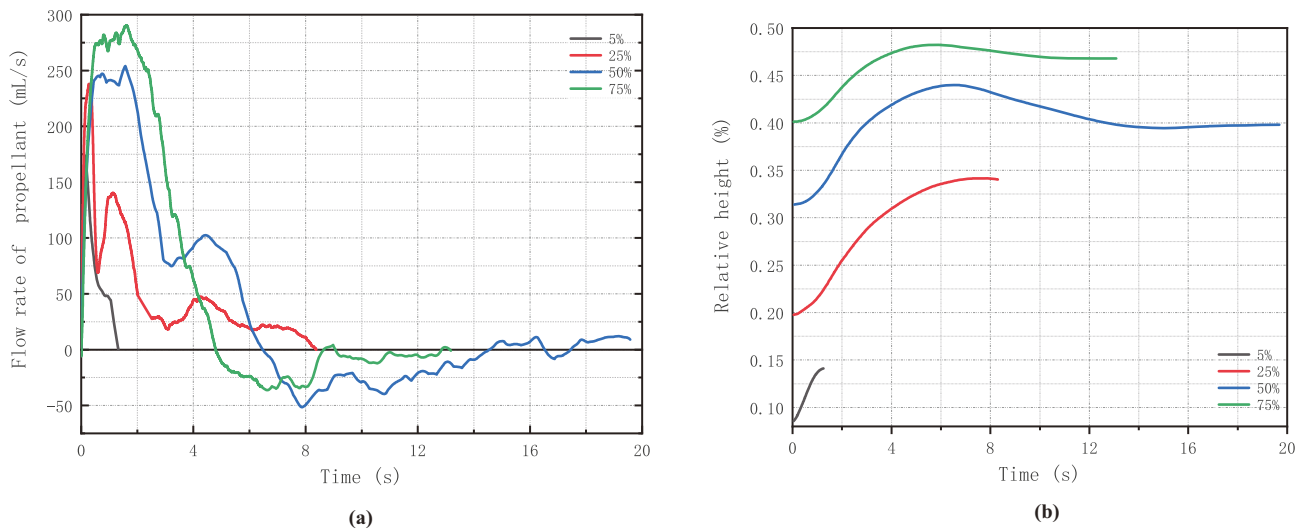


Fig. 10 Flow rate curve and mass center curve under Lateral acceleration

time curve and mass center/time curve, the reorientation process can be divided into two stages: the mutational stage and the stable stage, just the same as the result in the ref. (Zhuang et al. 2020). In the mutational stage, the flow rate changes a lot, and the mass center increases rapidly. In the stable stage, the flow rate oscillates around zero, and the mass center keeps unchanged almost.

Because the maximum flow rate is determined by the potential energy of liquid that increases with the liquid volume augmenting, the maximum flow rate at a high fill ratio will keep a high level and a longer time, which can be clearly seen in (Figs. 7, 8, 9, 10) focusing on the difference

among fill ratios under the same acceleration condition. The number of peaks and troughs of flow rate curves represents the degree of liquid sloshing, i.e. the smooth curve means the stable relocation process. Thus, it can be approved in (Figs. 7, 8, 9, 10) that the reorientation process is more stable at the fill ratio of 5% or 75%, and the reorientation process is more unstable at the fill ratio of 25% or 50%. The stability determines the completion time of the reorientation process. From the variation trend of the mass center in (Figs. 7, 8, 9, 10), it can be found that the variation trend of the mass center obeys the rule that a large volume liquid has a high mass center, except for the reverse & lateral condition

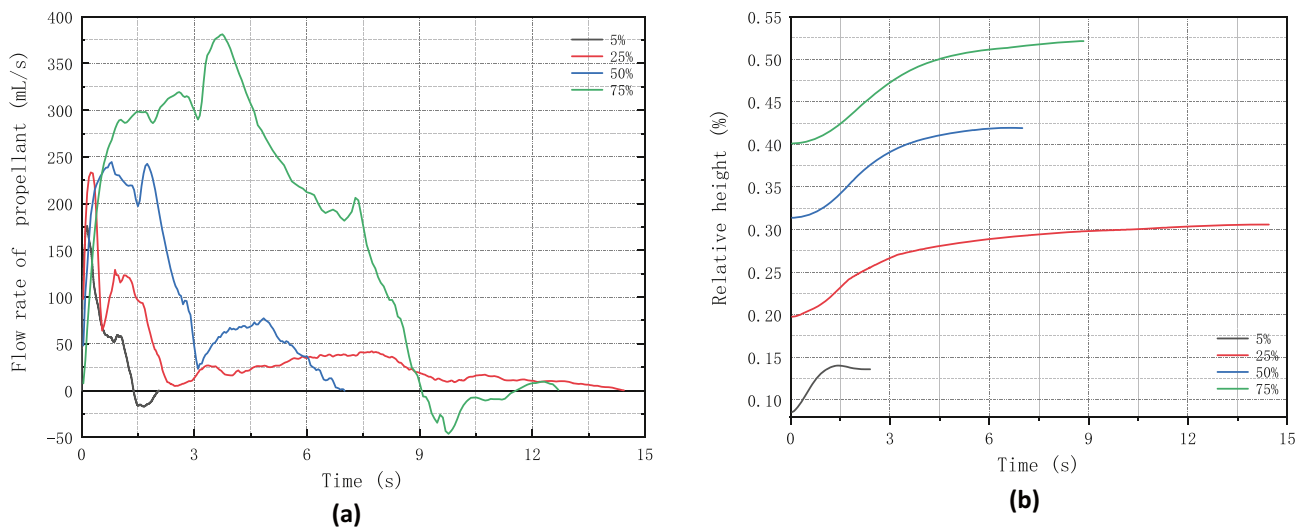


Fig. 11 Flow rate curve and mass center curve under rotation condition

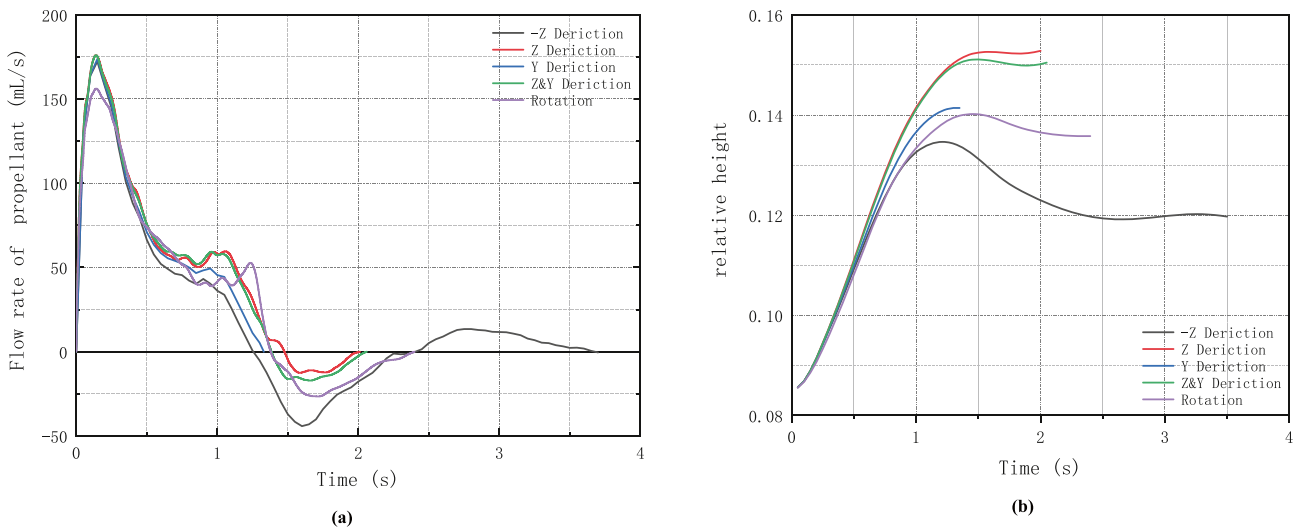


Fig. 12 Flow rate curve and mass center curve at 5% fill ratio

and the reverse condition. That is because of the influence of the force in the Z direction. When the liquid volume is large enough to escape the absorption of the sponges, the mass center of different volume liquid will no longer be decided by the fill ratio. By comparing the flow rate curve and mass center curve in (Figs. 12, 13, 14, 15), it can be found that the curve trend is similar under the reverse & lateral condition and the reverse condition, but different under the lateral condition. Even though the reverse & lateral condition is the combination of the reverse condition and lateral condition. That means the entire reorientation process under the reverse & lateral condition is mainly dominated by the acceleration in the Z direction rather than the the acceleration in Y or X

direction. It can also be proved by the later dynamic analysis. It can be found that the mass center is associated with the flow rate from (Figs. 7, 8, 9, 10, 11, 12, 13, 14, 15). When the flow rate has a great change the slope of the mass center curve will also change. So, it can be concluded that the mass center curve is the joint effect of the initial mass center and the integral of the flow rate of the propellant.

Dynamic Analysis of Different Conditions

As the dynamic analysis can provide more information about sloshing intensity in different conditions, the surface integral force acting on the walls in different directions was

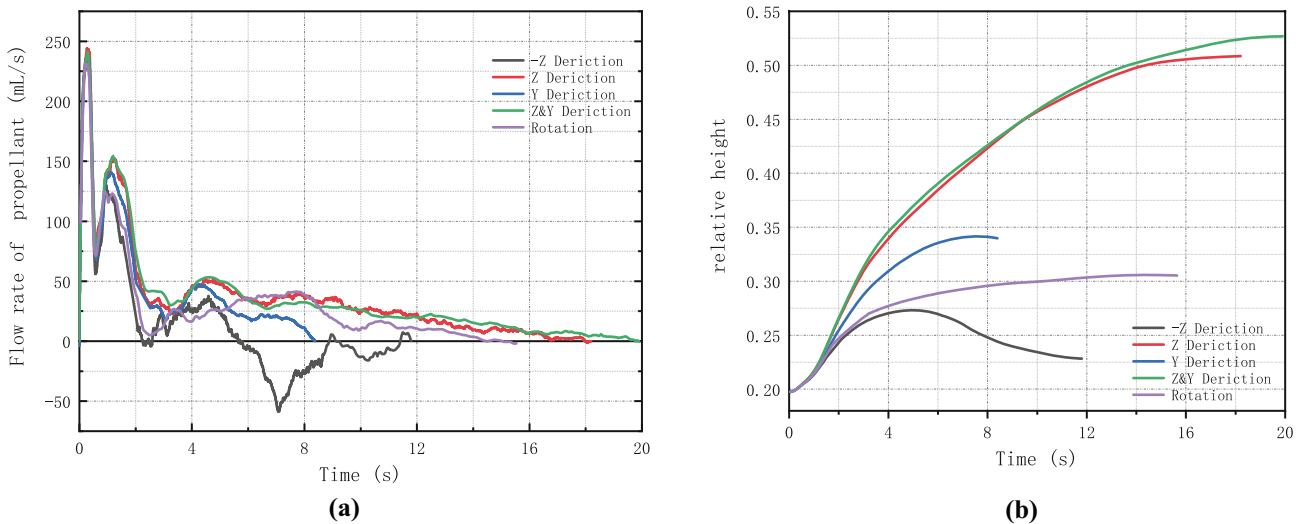


Fig. 13 Flow rate curve and mass center curve at 25% fill ratio

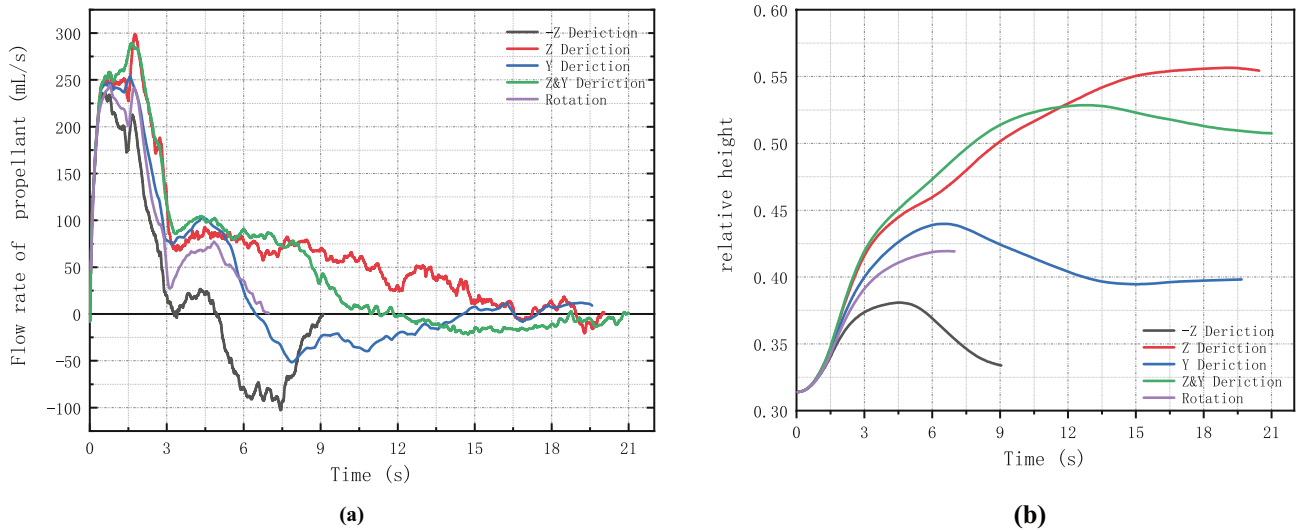


Fig. 14 Flow rate curve and mass center curve at 50% fill ratio

abstracted. The walls contain the tank shell, vanes, panels, and other widgets. The vane-type tank in this study is axial symmetry, so the force in the Y direction and the X direction will be similar under the bottom condition, the reverse condition, and the rotation condition. Among all simulation conditions, only the acceleration in the Y direction was not contained. For the convenience of comparison, the force in the Z direction and the Y direction was monitored to get more details about the propellant sloshing and the dynamic in different conditions.

By analyzing the magnitudes of the force in the Z direction and the Y direction in (Figs. 16, 17, 18, 19, 20), it can

be clearly seen that the force in the Z direction is bigger than the force in the Y direction, and the force in the Y direction change more frequently around the zero. That means the force in the Z direction is the main driving force for the propellant movement, which verifies the ability of PMD in liquid control and liquid communication. As there is no PMD arranged and no acceleration in the Y direction, the propellant sloshing always happens in the Y direction. The force in the Y direction under different conditions is almost similar, but we can still find that the force at the fill ratio of 5% or 75% will be smaller than the force at the fill ratio of 25% or 50%. The force in the Z direction has clear different patterns at

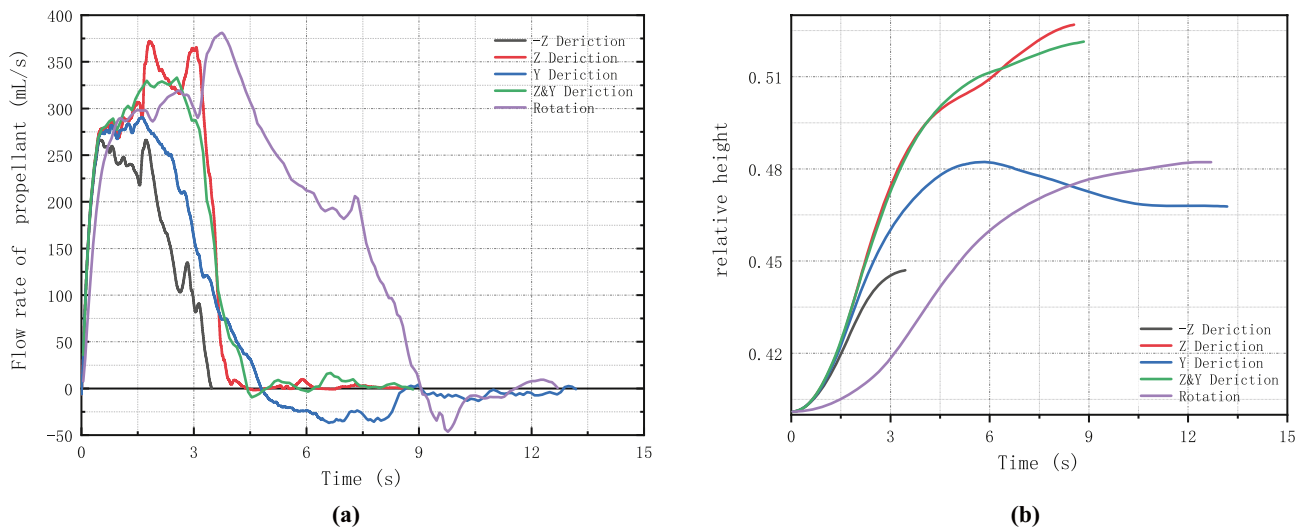


Fig. 15 Flow rate curve and mass center curve at 75% fill ratio

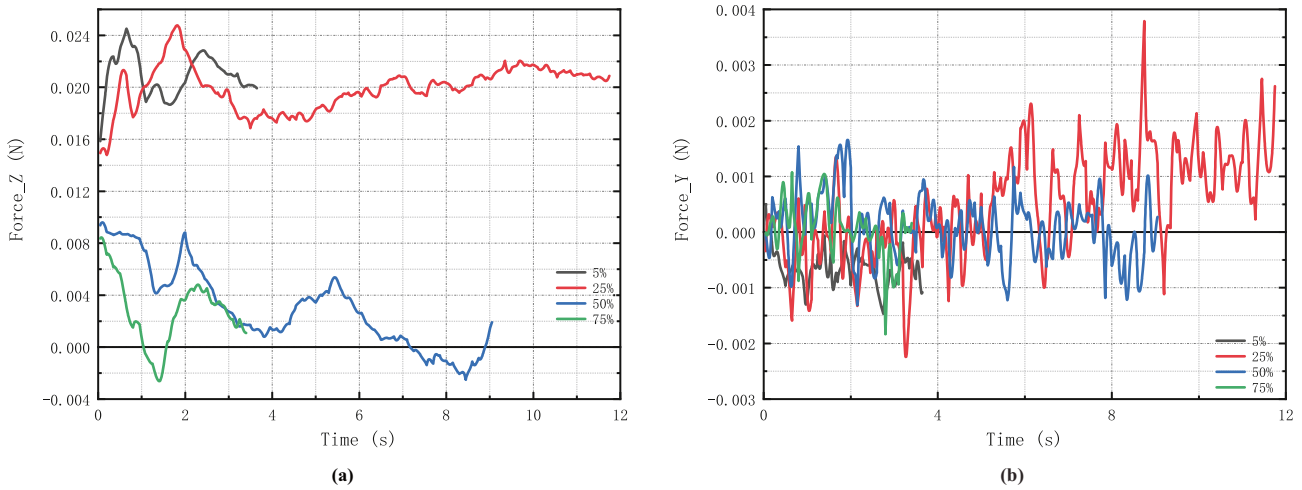


Fig. 16 Force at Z direction and Y direction under bottom acceleration

different fill ratios. If we consider the force without direction only with the value, the fill ratio is bigger when the force is smaller. Moreover, the force variation trends at the fill ratio of 5% and 25% seem to be opposite to that at the fill ratio of 50% and 75% because of the change of the main phase in the tank. Something more interesting that can be found is that there seems to be an asymptotic line between the fore at the fill ratio of 5% and 25%, and the fore at the fill ratio of 50% and 75% at the same acceleration. The value of the asymptotic line is similar under the sink condition and the reverse condition. And the values under the condition of lateral acceleration, lateral & reverse acceleration, and rotation is similar.

As the force in the Y direction has a slight difference, the force in the Z direction at the same fill ratio in different acceleration environments is further analyzed only. In, (Fig. 21) it can be clearly seen that variation trends of different acceleration environments at the same fill ratio are similar though the value of different acceleration conditions is different. And the difference between variation trends will be evident as the fill ratio increases. These phenomena clarify the great effect of fill ratios on the reorientation process. The acceleration conditions also influence the force in the Z direction. When the acceleration is in the Z or the minus Z direction, the force in the Z direction will reduce. Furthermore, the force curves at the fill ratio

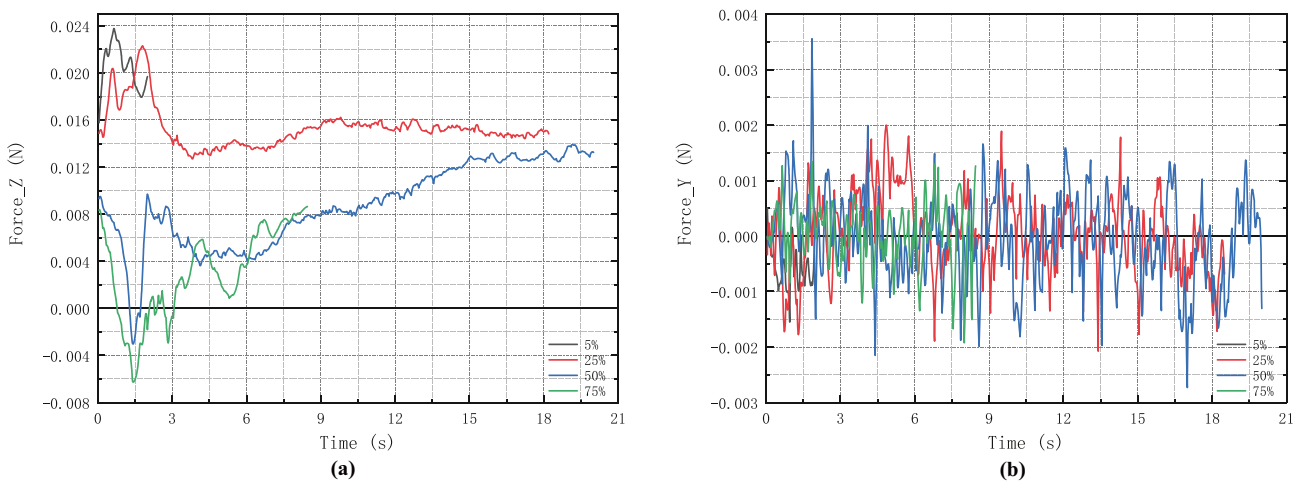


Fig. 17 Force at Z direction and Y direction under reverse acceleration

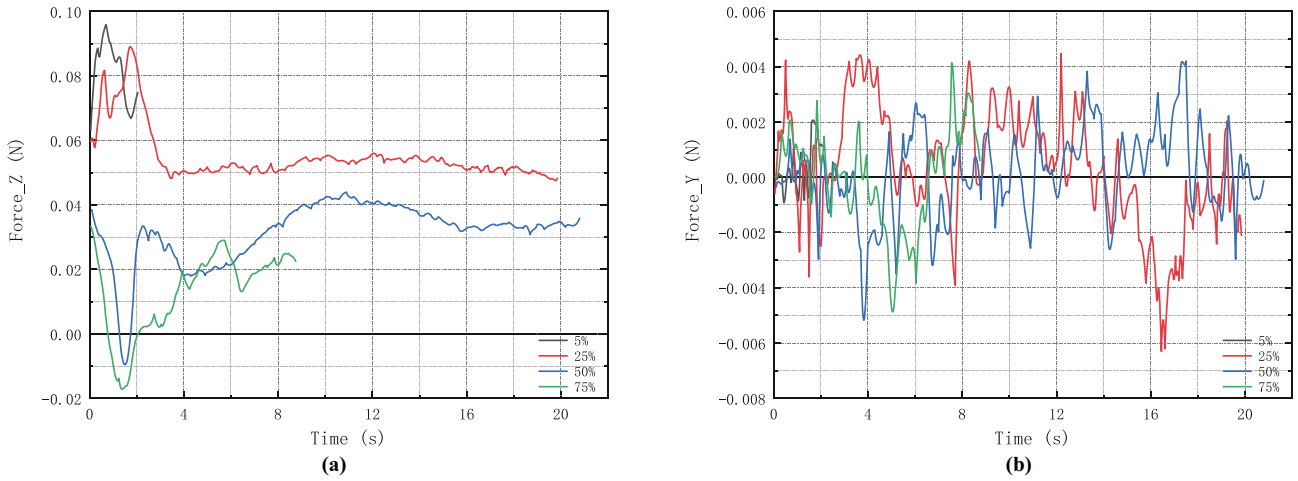


Fig. 18 Force at Z direction and Y direction at lateral&reverse acceleration

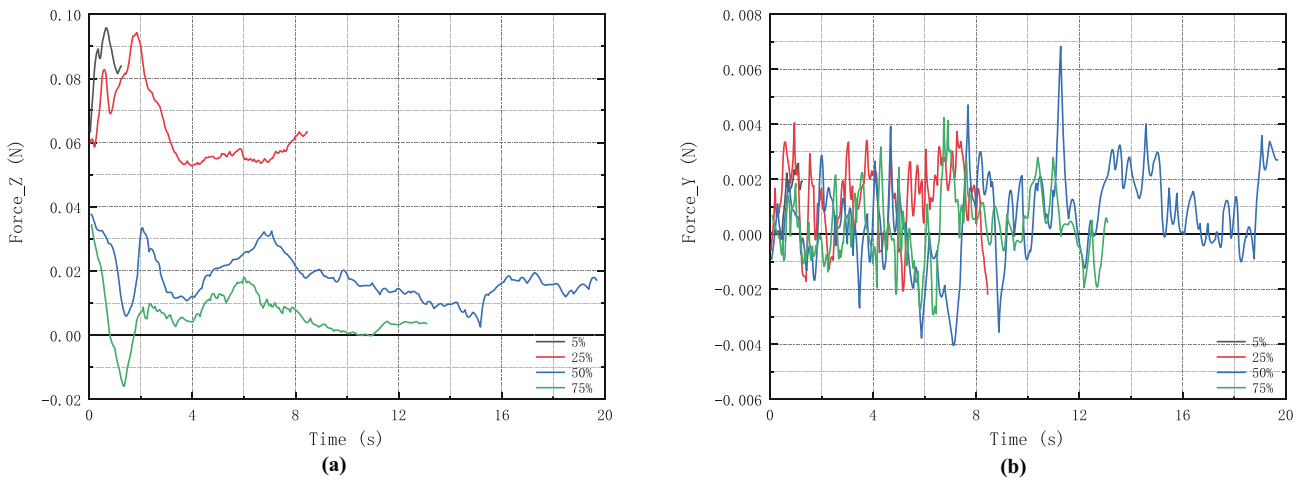


Fig. 19 Force at Z direction and Y direction under lateral acceleration

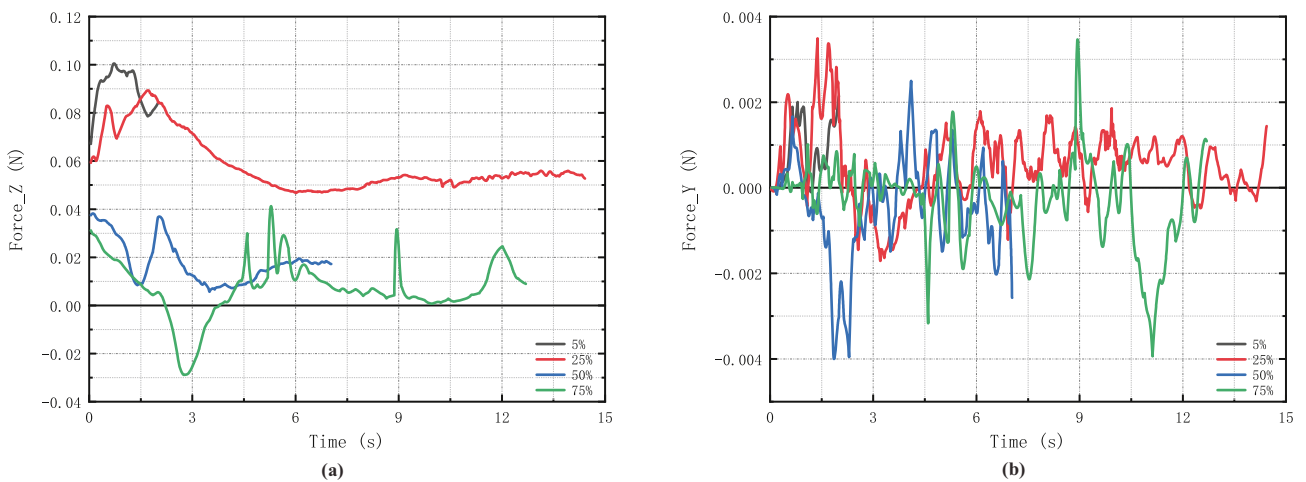


Fig. 20 Force at Z direction and Y direction under rotation condition

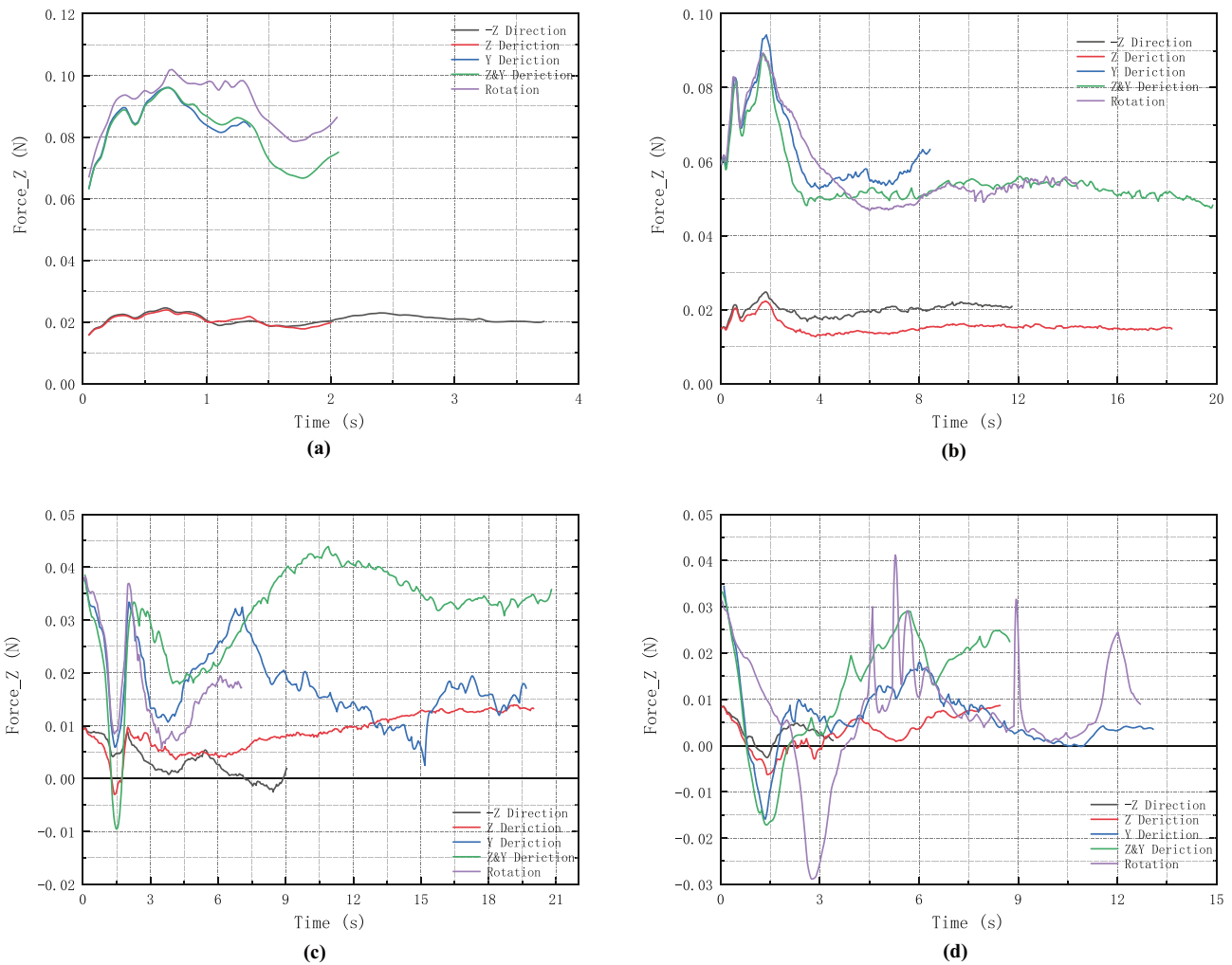


Fig. 21 Force at Z direction at different fill ratios

of 50% and 75% are more uneven than the force curves at the fill ratio of 5% and 25% due to the big density and inertance of liquid.

Conclusion

The reorientation process under the bottom condition, the lateral condition, the reverse condition, the reverse & lateral condition, and the rotation condition with different propellant volume fill ratios were simulated by commercial software Ansys Fluent with the VOF model. The different effects of the various acceleration environments and fill ratios have been analyzed. From the comparison of various gas–liquid contours and gas–liquid interfaces, it can be concluded that the forms of the air cavity at the end of the reorientation process are determined by the

joint effect of PMD, propellant volume fill ratio, and the acceleration condition. When the propellant is close to the vanes, the effect of PMD dominates, and this phenomenon can be obviously observed at 5% fill ratio by analyzing the contour and the interface form. However, when the propellant is far from the vanes the effect of the acceleration environment will dominate, such as the simulation results at the fill ratio of 75%. According to the volume flow rate through the initial gas–liquid interface, the reorientation process can be divided into two stages: the mutational stage and the stable stage. To analyze the intensity of liquid sloshing, the flow rate through the initial gas–liquid interface, mass center, and dynamic analysis at different directions during the reorientation process of all simulation conditions are compared. In terms of the volume fill ratio, sloshing will strengthen at the medium fill ratio, such as 25% fill ratio and 50% fill ratio. In terms

of the acceleration environment, the sloshing intensity will decrease under the bottom condition and the reverse condition. With the sloshing strengthening, it will need more time to finish the reorientation process. Worse still, it may break the balance between the gas and liquid and make the entire system break down. So, we need to pay more attention to these conditions both in the process of designing and testing to ensure a steady operation of the entire system. The force variation trend is influenced by the joint effect of fill ratios and acceleration environments. The value of force at the Z-axis gets smaller as the fill ratio gets bigger. There is an approximate asymptotic line between the curves of fore at the fill ratio of 5% and 25%, and the fill ratio of 50% and 75%. And the value of the asymptotic line is influenced by the acceleration condition. The smooth mass center curve and the clear gas–liquid interface mean the total reorientation process of all simulations is stable. It can be proved that this kind of vane-type propellant tank can provide a gas-free propellant for thrusters in space with this gravity level. This study can give guidance to the future design of the vane-type surface tension tank.

Acknowledgements This study was financially supported by Advanced Space Propulsion Laboratory of BICE and Beijing Engineering Research Center of Efficient and Green Aerospace Propulsion Technology, NO: LabASP-2021-03.

Declarations

Competing Interest The authors declare that they have no known competing financial interests or personal relationships that could have appeared to influence the work reported in this paper.

References

- Albadawi, A., Donoghue, D.B., Robinson, A.J., Murray, D.B., Delauré, Y.M.C.: On the assessment of a VOF based compressive interface capturing scheme for the analysis of bubble impact on and bounce from a flat horizontal surface. *Int. J. Multiph. Flow.* **65**, 82–97 (2014). <https://doi.org/10.1016/j.ijmultiphaseflow.2014.05.017>
- ANSYS, I.: ANSYS FLUENT User's Guide. (2012)
- Brackbill, J.U., Kothe, D.B., Zemach, C.: A continuum method for modeling surface tension. *J. Comput. Phys.* **100**, 335–354 (1992). [https://doi.org/10.1016/0021-9991\(92\)90240-Y](https://doi.org/10.1016/0021-9991(92)90240-Y)
- Bronowicki, P., Canfield, P., Grah, A., Dreyer, M.: Free surfaces in open capillary channels-Parallel plates. *Phys. Fluids.* **27**, (2015). <https://doi.org/10.1063/1.4906154>
- Chen, Y., Weislogel, M.M., Nardin, C.L.: Capillary-driven flows along rounded interior corners. **566**, (2006)
- Concus, P., Finn, R.: On the Behavior of a Capillary Surface in a Wedge. *Proc. Natl. Acad. Sci.* **63**, 292–299 (1969). <https://doi.org/10.1073/pnas.63.2.292>
- Dodge, F.T.: Further studies of low-gravity conditions by low-gravity conditions. (1971)
- Dong, M., Chatzis, I.: The Imbibition and Flow of a Wetting Liquid along the Corners of a Square Capillary Tube. *J. Colloid Interface Sci.* **172**, 278–288 (1995)
- Dowdy, M.W., Hise, R.E., Peterson, R.G.: Development and qualification of the propellant management system for viking 75 orbiter. *J. Spacecr. Rockets.* **14**, 133–140 (1977). <https://doi.org/10.2514/3.57172>
- Gueyffier, D., Li, J., Nadim, A., Scardovelli, R., Zaleski, S.: Volume-of-Fluid Interface Tracking with Smoothed Surface Stress Methods for Three-Dimensional Flows. *J. Comput. Phys.* **152**, 423–456 (1999). <https://doi.org/10.1006/jcph.1998.6168>
- Hartwig, J.W.: Optimal Propellant Management Device for a Small-Scale Liquid Hydrogen Propellant Tank. *Liq. Acquis. Devices Adv. In-sp. Cryog. Propuls. Syst.* 343–369 (2016). <https://doi.org/10.1016/b978-0-12-803989-2.00014-0>
- Hartwig, J.W.: Propellant management devices for low-gravity fluid management: Past, present, and future applications. *J. Spacecr. Rockets.* **54**, 808–824 (2017). <https://doi.org/10.2514/1.A33750>
- Hibbard, R.L.: Satellite on-orbit refueling: acoust effectiveness analysis. (1996)
- Hirt, C.W., Nichols, B.D.: Volume of Fluid (VOF) Method for the Dynamics of Free Boundaries. *J. Comput. Phys.* **39**, 201–225 (1981). <https://doi.org/10.1007/s40998-018-0069-1>
- Hu, Q., Li, Y., Liang, J., Liu, J., Song, T.: Liquid Sloshing Performance in Vane Type Tank under Microgravity. *Aerosp. Control.* **35**, 19–24 (2017). <https://doi.org/10.1088/1757-899X/129/1/012016>
- Huang, B., Wang, L., Chen, L., Liu, J., Wu, D.: Analysis of propellant sloshing behavior in vane type surface tension tank in lateral microgravity environment. *Aerosp. Control. Appl.* **47**, 63–69 (2021).
- Jaekle, D.E.: Propellant Management Device Conceptual Design and Analysis - Vanes. (1991). <https://doi.org/10.2514/6.1991-2172>
- Ibrahim, R.A., Pilipchuk, V.N., Ikeda, T.: Recent advances in liquid sloshing dynamics. *Appl. Mech. Rev.* **54**, 133–199 (2001). <https://doi.org/10.1115/1.3097293>
- Jaekle, D.E.: Propellant Management Device Conceptual Design and Analysis - Sponges. (1993). <https://doi.org/10.2514/6.1993-1970>
- Jaekle, D.E.: Propellant management device conceptual design and analysis: Galleries. 33rd Jt. Propuls. Conf. Exhib. (1997). <https://doi.org/10.2514/6.1997-2811>
- Kang, Q., Hou, R., Duan, L., Hu, L.: Capillary flow along rounded interior corner of right angle under microgravity. In: *ICEM 2008: Int. Conf. Exp. Mech.* **7375**, (2008)
- Kartuzova, O., Kassemi, M.: Modeling interfacial turbulent heat transfer during ventless pressurization of a large scale cryogenic storage tank in microgravity. 47th AIAA/ASME/SAE/ASEE Jt. Propuls. Conf. Exhib. 1–18, (2011). <https://doi.org/10.2514/6.2011-6037>
- Kartuzova, O., Kassemi, M.: Modeling ullage dynamics of tank pressure control experiment during jet mixing in microgravity. 52nd AIAA/SAE/ASEE Jt. Propuls. Conf. **19**, 1–15 (2016). <https://doi.org/10.2514/6.2016-4677>
- Lenormand, R., Zarcone, C.: Role of Roughness and Edges During Imbibition in Square Capillaries. *Soc. Pet. Eng. AIME, SPE.* (1984). <https://doi.org/10.2118/13264-ms>
- Li, Y., Pan, H., Wei, Y.: The Evolvement of the Study and Application on the Second Generation Surface Tension Tank. *J. Astronaut.* **28**, 503–507 (2007)
- Hastings, L.J., Reginald III, R.: Low gravity liquid-vapor interface shapes in axisymmetric containers and a computersolution. (1968)
- Liu, J., Li, Y., Li, W., Zhuang, B., Zhou, C.: Experimental investigation of liquid transport in a vane type tank of satellite with microgravity. *Aerosp. Sci. Technol.* **105**, 106007 (2020). <https://doi.org/10.1016/j.ast.2020.106007>
- Michael, D.H.: Meniscus Stability. *Annu. Rev. Fluid Mech.* **13**, 189–216 (1981). <https://doi.org/10.1146/annurev.fl.13.010181.001201>

- Peterson, R.G.: Surface tension propellant control for Viking 75 Orbiter. (1976). <https://doi.org/10.2514/6.1976-596>
- Rollins, J.R., Grove, R.K., Jaekle, D.E.: Twenty-Three Years of Surface Tension Propellant Management System - Design, Development, Manufacture, Test, and Operation. AIAA Pap. (1985). <https://doi.org/10.2514/6.1985-1199>
- Rosendahl, U., Grah, A., Dreyer, M.E.: Convective dominated flows in open capillary channels. *Phys. Fluids*. **22**, 1–13 (2010). <https://doi.org/10.1063/1.3379847>
- Saltari, F., Traini, A., Gambioli, F., Mastroddi, F.: A linearized reduced-order model approach for sloshing to be used for aerospace design. *Aerosp. Sci. Technol.* **108**, 106369 (2021). <https://doi.org/10.1016/j.ast.2020.106369>
- Shin, S., Lee, W. II: Finite element analysis of incompressible viscous flow with moving free surface by selective volume of fluid method (2000)
- Silva, M.C.F., Campos, J.B.L.M., Miranda, J.M., Araújo, J.D.P.: Numerical study of single Taylor bubble movement through a microchannel using different CFD packages. *Processes*. **8**, 1–19 (2020). <https://doi.org/10.3390/pr8111418>
- Srinivasan, R.: Estimating zero-g flow rates in open channels having capillary pumping vanes. *Int. J. Numer. Methods Fluids*. **41**, 389–417 (2003). <https://doi.org/10.1002/flid.446>
- Stark, J.A., Bradshaw, R.D., Blatt, H.M.: Low-g fluid behavior technology summaries. (1974)
- Stuparu, A., Susan-Resiga, R., Bosioc, A.: CFD simulation of solid suspension for a liquid–solid industrial stirred reactor. *Appl. Sci.* **11**, (2021). <https://doi.org/10.3390/app11125705>
- Tam, W., Ballinger, I., Jaekle Jr., D.: Tank Trade Study - An Overview. 44th AIAA/ASME/SAE/ASEE Jt. Propuls. Conf. Exhib. (2008). <https://doi.org/10.2514/6.2008-4940>
- Thibaut, A., Cheuret, F., Marraffa, L.: Numerical and experimental investigation on the interface shape of cryogenic fluids in microgravity and spinning conditions. In: 7th Eur. Symp. Aerothermo. (2011)
- Veldman, A.E.P., Gerrits, J., Luppens, R., Helder, J.A., Vreeburg, J.P.B.: The numerical simulation of liquid sloshing on board spacecraft. *J. Comput. Phys.* **224**, 82–99 (2007). <https://doi.org/10.1016/j.jcp.2006.12.020>
- Wei, Y.: Research on the Flow in the Process of the Propellant Management in a Spacecraft Tank Under Microgravity (2013)
- Weislogel, M.M.: Capillary flow in interior corners: The infinite column. *Phys. Fluids*. **13**, 3101–3107 (2001). <https://doi.org/10.1063/1.1408918>
- Weislogel, M.M., Lichter, S.: Capillary flow in an interior corner. *J. Fluid Mech.* **373**, 349–378 (1998). <https://doi.org/10.1017/S0022112098002535>
- Wu, Z., Huang, Y., Chen, X., Zhang, X.: Capillary-driven flows along curved interior corners. *Int. J. Multiph. Flow*. **109**, 14–25 (2018). <https://doi.org/10.1016/j.ijmultiphaseflow.2018.04.004>
- Wu, Z., Huang, Y., Chen, X., Zhang, X., Yao, W.: Flow rate limitation in curved open capillary groove channels. *Int. J. Multiph. Flow*. **116**, 164–175 (2019). <https://doi.org/10.1016/j.ijmultiphaseflow.2019.03.016>
- Yang, H.Q., Peugeot, J.: Propellant sloshing parameter extraction from computational-fluid-dynamics analysis. *J. Spacecr. Rockets*. **51**, 908–916 (2014). <https://doi.org/10.2514/1.A32608>
- Zhuang, B., Li, Y., Liu, J., Rui, W.: Numerical Simulation of Fluid Transport along Parallel Vanes for Vane Type Propellant Tanks. *Microgravity Sci. Technol.* **32**, 129–138 (2020). <https://doi.org/10.1007/s12217-019-09746-2>

Publisher's Note Springer Nature remains neutral with regard to jurisdictional claims in published maps and institutional affiliations.